ARCTIC
VOL. 74, NO. 3 (SEPTEMBER 2021) P. 339–354
https://doi.org/10.14430/arctic73377

Daily Field Observations of Retrogressive Thaw Slump Dynamics in the Canadian High Arctic

Melissa K. Ward Jones[1] and Wayne H. Pollard[2]

(*Received 24 July 2020; accepted in revised form 15 March 2021*)

ABSTRACT. With observed increases in retrogressive thaw slump (RTS) number, rates, and size in recent decades, there is a need to understand these highly dynamic landforms as they impact surrounding ecosystems and infrastructure. There is a general lack of detailed (e.g., daily) field observations of change in RTSs; we help fill this gap by monitoring three RTSs for much of the 2017 thaw period by setting up and tracking survey transects on a near daily basis. We correlated mean daily and cumulative retreat to mean daily air temperature (MDAT), total daily precipitation (TDP), and cumulative thawing degree days (TDD) using various polynomial regressions and Pearson correlation techniques. Our results show that July retreat was highly variable, and periods of increased RTS retreat did not always align with periods of increased air temperature. Also, multiple periods of increased retreat largely driven by sediment distribution in the RTS floor could occur within a single period of increased air temperature. Retreat rates decreased suddenly in early August, indicating a threshold of either air temperature, solar radiation or a combination of both must be reached for increased retreat rates. A statistically significant correlation was found between daily mean and mean cumulative retreat with MDAT ($p > 0.001$) and TDD ($p > 0.001$ and > 0.0001) but not with total daily precipitation. Correlating mean cumulative retreat and TDD using polynomial regression generated R^2 values greater than 0.99 for all three sites. Both cumulative retreat and TDD account for past and current conditions, as well as lag responses, within the monitoring period. The high R^2 values for the correlation of mean cumulative retreat and TDD suggest the potential for accurately modelling RTS retreat with minimal field data (air temperature and headwall position), however modelling is currently restricted to individual RTSs and only within short time scales. Monitoring RTSs on a daily scale allows RTS behaviour and trends to be identified that may be obscured at annual time scales and highlights the importance of all system inputs when considering RTS retreat dynamics.

Key words: Arctic; permafrost; thermokarst; retrogressive thaw slumps; climate change; Fosheim Peninsula; Ellesmere Island

RÉSUMÉ. Compte tenu du nombre, des taux et de la taille à la hausse des glissements rétrogressifs dus au (GRD) dégel au cours des dernières décennies, il y a lieu de comprendre ces reliefs fortement dynamiques, car ils ont des impacts sur les infrastructures et les écosystèmes environnants. Il y a un manque général d'observations détaillées (c'est-à-dire quotidiennes) sur le terrain en ce qui a trait aux GRD. Nous aidons à combler cet écart grâce à la surveillance de trois GRD pendant une grande partie de la période de dégel de 2017 en dressant des transects et en en faisant des suivis presque au quotidien. Nous avons corrélé le recul quotidien et cumulatif moyen à la température moyenne quotidienne de l'air (TMQA), aux précipitations totales quotidiennes (PTQ) et aux degrés-jours de dégel cumulés (DJD) à l'aide de diverses régressions polynomiales et des techniques de corrélation de Pearson. Nos résultats indiquent que le recul du mois de juillet variait considérablement, et que les périodes de recul accru des GRD ne coïncidaient pas toujours avec les périodes de température à la hausse de l'air. Par ailleurs, de multiples périodes de recul accru largement attribuables à la distribution des sédiments dans le fond des GRD pouvaient se produire au cours d'une seule période de température de l'air à la hausse. Au début d'août, les taux de recul ont diminué soudainement, ce qui indiquait qu'un seuil de température de l'air ou un seuil de rayonnement solaire, ou encore, qu'un ensemble des deux doit être atteint pour donner lieu à des taux de recul plus élevés. Une corrélation statistiquement significative a été trouvée entre le recul moyen quotidien et le recul moyen quotidien cumulé avec la TMQA ($p > 0{,}001$) et les DJD ($p > 0{,}001$ et $> 0{,}0001$), et non pas avec les précipitations totales quotidiennes. La corrélation du recul moyen cumulé et des DJD à l'aide de la régression polynomiale a généré des valeurs R^2 supérieures à 0,99 aux trois sites. Tant les reculs cumulés que les DJD tiennent compte des conditions antérieures et actuelles, ainsi que des décalages, à l'intérieur de la période de surveillance. Les valeurs R^2 élevées propres à la corrélation du recul moyen cumulé et des DJD suggèrent des possibilités de modélisation exacte du recul des GRD moyennant des données minimales prélevées sur le terrain (température de l'air et position du mur de rimaye). Cependant, en ce moment, la modélisation est restreinte aux GRD individuels, et seulement à l'intérieur d'échelles de temps réduites. La surveillance des GRD sur une échelle journalière permet de cerner les

[1] Corresponding author: Institute of Northern Engineering, 1764 Tanana Loop, University of Alaska Fairbanks, Fairbanks, Alaska 99775-5910, USA; mkwardjones@alaska.edu
[2] Department of Geography, 805 Sherbrooke Street West, McGill University, Montreal, Quebec H3A 0B9, Canada

comportements et les tendances des GRD, ceux-ci pouvant être éclipsés dans le cadre d'échelles annuelles. La surveillance met également en évidence l'importance de tous les intrants du système dans la considération de la dynamique du recul des GRD.

Mots clés : Arctique; pergélisol; thermokarst; glissements rétrogressifs dus au dégel; changement climatique; péninsule Fosheim; île d'Ellesmere

Traduit pour la revue *Arctic* par Nicole Giguère.

INTRODUCTION

Retrogressive thaw slumps (RTSs) are dynamic landforms created by degrading ice-rich permafrost (Kokelj and Jorgensen, 2013). These mass-wasting, horseshoe- or cusp-shaped features grow by an ablating ice-rich headwall where the fluidized sediments that pool at the base of the headwall flow downslope along the RTS floor. These features have been observed to impact infrastructure (Van der Sluijs et al., 2018) as well as aquatic and terrestrial ecosystems from the release of sediments and solutes (Kokelj and Lewkowicz, 1999; Mesquita et al., 2010, Kokelj et al., 2013, 2017; Malone et al., 2013) by inducing change in vegetation communities (Lantz et al., 2009; Thienpont et al., 2013; Cray and Pollard, 2015) and ground temperatures (Burn, 2000). These "pulse disturbances" (Grosse et al., 2011; Liljedahl, 2016) can remain active for decades (Lacelle et al., 2015) or stabilize within a period of only a few years (Ward Jones et al., 2019). Polycyclic RTSs are generated when a new thaw face develops within the area of an existing or stabilized RTS (Lantuit and Pollard, 2008).

RTSs can develop in response to local processes such as slope instability (e.g., active layer detachments; e.g., Swanson, 2021), coastal erosion (e.g., Lantuit and Pollard, 2008; Obu et al., 2017; Ramage et al., 2017), or erosional processes such as gullying (e.g., Bowden et al., 2008). Their widespread increase in activity can be indicative, however, of more widespread systematic changes within a region from extreme weather events or climate (e.g., Lewkowicz and Way, 2019; Ward Jones et al., 2019). Such widespread increases have been observed in various parts of the Arctic in recent decades (Lantz and Kokelj, 2008; Kokelj et al., 2015, 2017; Lacelle et al., 2015; Segal et al., 2016; Khomutov et al., 2017; Lewkowicz and Way, 2019; Ward Jones et al., 2019). Mapping of RTS sites in northwestern Canada showed that 17% of a 1,274,625 km^2 area contained RTS-affected terrain (Kokelj et al., 2017); on Banks Island, 4000 RTSs were initiated between 1984 and 2015 (Lewkowicz and Way, 2019). Measured retreat rates of RTS range up to 38 m/yr in the Noatak Valley of Alaska (Swanson and Nolan, 2018), mean retreat ranges between 7.2 m/yr and 26.7 m/yr in northwestern Canada (De Krom and Pollard, 1989; Lantuit and Pollard, 2008; Lacelle et al., 2015) and between 2.51 m/yr and 14 m/yr in the Canadian High Arctic on Ellesmere Island (Burn and Lewkowicz, 1990; Robinson, 2000; Grom and Pollard, 2008; Ward Jones et al., 2019). Not only are RTS numbers increasing but the overall observed size is also increasing; RTSs 20 ha or greater, known as "megaslumps" have been introduced in the scientific literature in recent years (Günther et al., 2015; Kokelj et al., 2015, 2017; Lacelle et al., 2015; Murton et al., 2017). To date, these have only been observed in the low Arctic (Ward Jones et al., 2019).

One of the difficulties in advancing our understanding of RTS dynamics is the limited detailed field observations, which results in assumptions or generalizations made in the interpretation of their dynamics. We monitored three RTSs daily during the 2017 thaw season to explore RTS responses to mean daily air temperature (MDAT), total daily precipitation (TDP), and thawing degree days (TDD) as well as terrain factors such as sediment distribution in the RTS floor to gain additional insights on a sub-seasonal scale to help our understanding of RTS activity. We compare statistical correlations between mean daily retreat and mean cumulative retreat to MDAT, TDP, and TDD to explore which variable correlation is optimal to help inform future research efforts.

Study Site

This research was conducted on three RTS sites within 5 km of the Eureka Weather Station, located on the Fosheim Peninsula, Ellesmere Island, Nunavut, Canada (Fig. 1; Table 1). These sites are near the coast but are not impacted by coastal erosion processes. This area has a polar desert climate with a mean annual, January, and July air temperatures of −19.7˚C, −36.1˚C, and +5.4°˚C, respectively, as measured by the Eureka Weather Station. Permafrost is over 500 m thick, has a −16.5˚C ground temperature at the depth of zero annual amplitude (at ~15.4 m depth), and is ice-rich in the upper 20–30 m (Pollard et al., 2015). Ground ice in this area consists of extensive pore ice, thinner layers of segregated ice, as well as extensive intrasedimental tabular massive ice and ice wedges (Pollard, 2000). Massive ice is found below Holocene marine limit (~148 m above sea level [asl]), although ice wedges are also found in unconsolidated materials above the marine limit (Pollard and Bell, 1998). Mean active layer depth is 57 cm (Couture and Pollard, 2007). Vegetation cover is patchy, and areas of bare soil are common (Couture and Pollard, 2007). Organic cover is sparse, thin, and locally distributed (Garneau, 2000).

Past RTS studies by Robinson (2000), Grom and Pollard (2008), Pollard et al. (2015), and Ward Jones and Pollard (2018) have focused on individual RTSs. These observations are either limited to longer time observation intervals such as weekly (Robinson, 2000) or annually (Pollard et al., 2015) or to short monitoring periods (~2 weeks, Grom

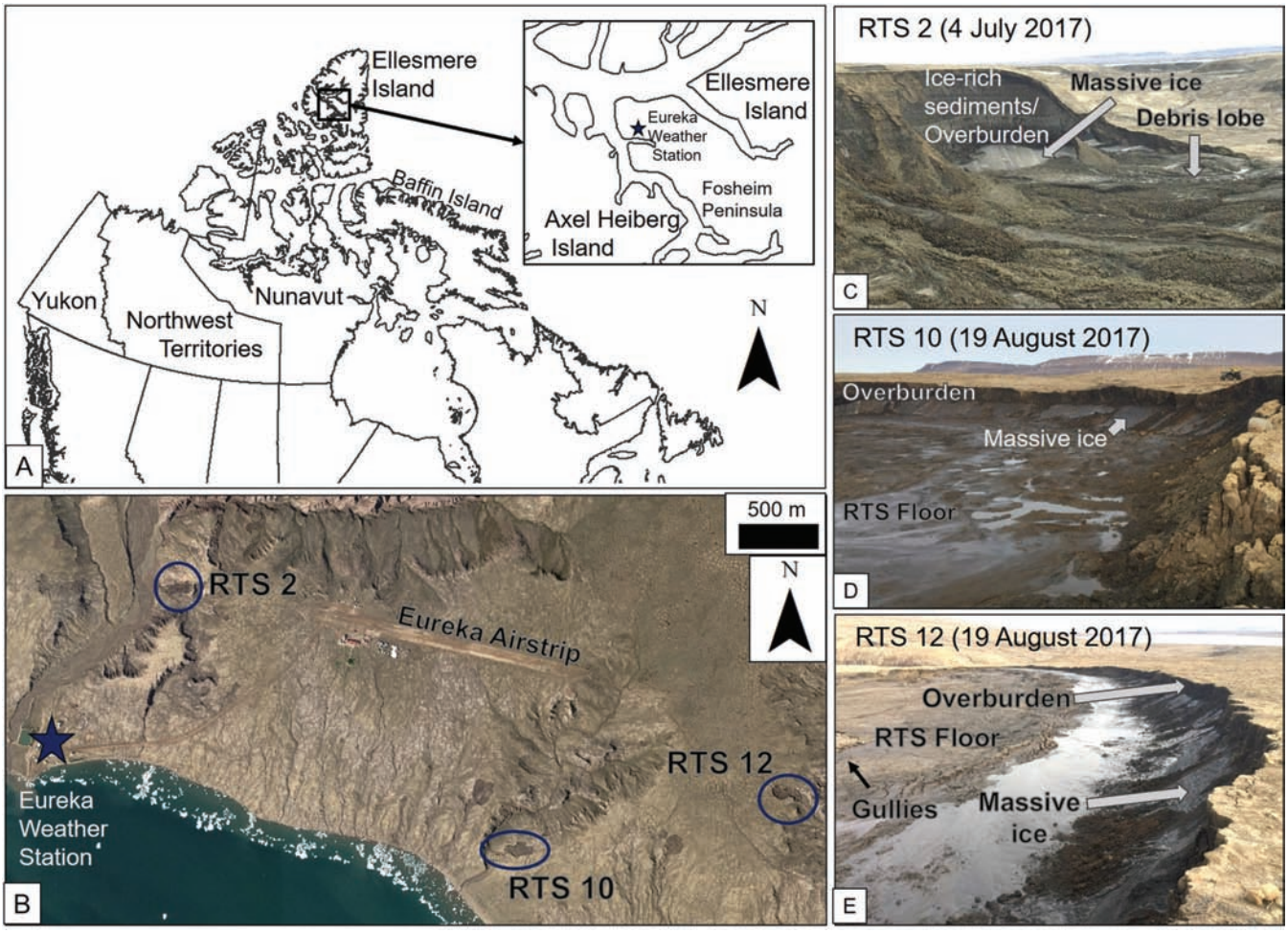

FIG. 1. (A) The location of the Fosheim Peninsula within the Canadian Arctic Archipelago. (B) Dark blue star denotes the location of the Eureka Weather Station and blue circles denote the location of each retrogressive thaw slump (RTS) site within a 2017 Worldview 3 image (© Maxar Technologies). (C), (D) and (E) show fields photos of RTS 2, 10, and 12, respectfully.

TABLE 1. RTS activity and terrain characteristic summary.

RTS	Year initiated[1]	Mean 2016–17 retreat[1] (m)	Mean 2017–18 retreat[1] (m)	Primary aspect[1] (°)	Mean headwall height (m; measured in 2018)	Mean overburden height (m; measured in 2017)	Volumetric ground ice content of tabular massive ice[2]
RTS 2	2011	4.3	2.4	268	17.2	10 m	93.1%
RTS 10	2011	2.0	0.8	251	2.0	92 cm	94.0% and 94.7%
RTS 12	2011	3.9	2.24	104	2.9	85 cm	71.0% and 57.0%

[1] Data from Ward Jones et al. (2019).
[2] Data from individual cores (Roy, 2019).

and Pollard, 2008). Ward Jones et al. (2019) focused both on local RTSs as well as RTS frequency counts annually at the landscape scale. Other geomorphic studies conducted in this area have focused on ice-wedge degradation (Hodgson and Nixon, 1998; Couture and Pollard, 2007; Pollard et al., 2015; Becker and Pollard, 2016; Becker et al., 2016; Bernard-Grand'Maison and Pollard, 2018; Ward Jones et al., 2020) as well as active layer detachment slides (Lewkowicz, 1990, 2007; Harris and Lewkowicz, 1993; Lewkowicz and Harris, 2005).

The RTSs included in this study are three (RTS 2, RTS 10, and RTS 12; Figs. 1 and 2; Table 1) of the 12 RTS sites from Ward Jones et al. (2019). Ward Jones et al. (2019) provided annual observations using either differential GPS (dGPS) mapping or high resolution remote sensing since RTS initialization in 2011 or 2012 until 2018. This study provides a data subset of daily observations from the 2017 field season. For consistency, we use the same site-naming scheme as Ward Jones et al. (2019). All three RTSs sites within this study were initiated in 2011 (Table 1). The overburden for each RTS consisted of fine grain sediments (silty clay to fine sand) of various thicknesses (Table 1). RTS 2 had the highest headwall at 17.2 m (measured in 2018; Table 1) and a 10.0 m thick overburden (Roy, 2019)

that included silty clay with thin layers of fine sand in the upper 1 m. Furthermore, the overburden consisted of a combination of reticulate ice and ice lenses only a few centimetres thick overlying tabular massive ice. Mean volumetric ice content of the massive ice was 93.1% (Roy, 2019). The primary aspect was west facing (268˚) and the slope of the surrounding undisturbed terrain was 5.2˚. Both RTS 10 and RTS 12 have smaller headwall heights (2.0 m and 2.9 m, respectively, as measured in 2018) and overburdens (92 cm and 85 cm, respectively; Table 1) overlying tabular massive ice intersected by wedge ice. There were no ice lenses within the overburdens of RTS 10 and RTS 12, and sediments consisted of silty clay. Mean volumetric ice content was 94% and 94.7% for RTS 10 and 71% and 57% for RTS 12 from two collected cores from each RTS within the tabular massive ice (Roy, 2019; Table 1). The slope of the surrounding undisturbed area for RTS 10 was 1.3˚ and primary aspect was west (251˚; Ward Jones et al., 2019; Table 1). For RTS 12, the slope of surrounding undisturbed terrain was 1.6˚ and primary aspect was east facing (104˚; Ward Jones et al., 2019).

METHODS

Field Monitoring and dGPS Mapping

In 2017, monitoring protocols were set up for RTS 2 on 29 June, for RTS 10 on 7 July, and for RTS 12 on 11 July; monitoring ended on 19 August for all three sites. Monitoring consisted of randomly placed transects of numbered and precisely located survey markers along the headwall containing exposed ground ice (Fig. 2). RTS sites were determined to be active as long as ground ice was visibly exposed. The flanks of each RTS became inactive overtime as each RTS grew in size and deposited sediments along those areas. Each RTS monitoring site had varying transect numbers, dependent on the amount of ground ice exposed along the headwall perimeter: RTS 2 had nine transects, RTS 10 had 15, and RTS 12 had 20 (Fig. 2). Each survey marker was numbered and spaced 30 cm apart along each transect. Each site was visited on a daily basis as per our field schedule. The survey marker number was recorded and an image taken of the RTS at each visit. On the last day of monitoring, the distance from the last marker to the edge of the headwall was measured. Retreat rates were determined by taking the number of days it took for the survey marker to fall into the slump over the 30 cm distance, meaning retreat measurements have a 30 cm resolution. Mean daily retreat was determined by taking the mean retreat of all transects within a given RTS. We denote retreat peaks as periods of mean retreat above the seasonal mean retreat (Fig. 3). Mean cumulative retreat was found by adding mean daily retreat rates for a given RTS site.

Survey marker locations were mapped using a Trimble 5700 dGPS during headwall mapping for Ward Jones et al. (2019). Collected rover points were post processed using

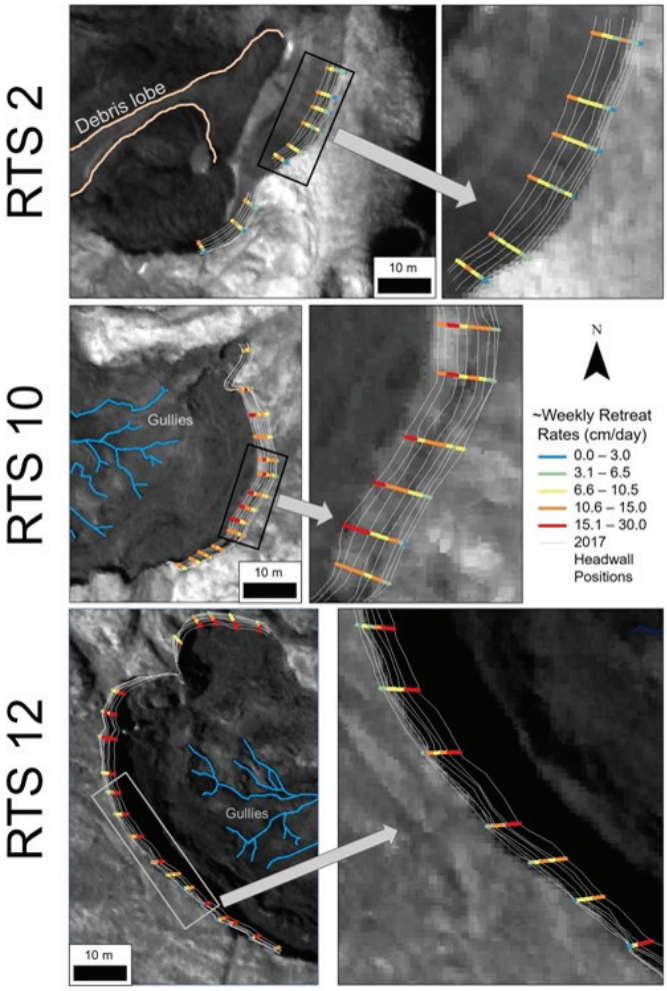

FIG. 2. Location of transects for RTS 2, 10, and 12 and weekly retreat rates using a 2017 Worldview 3 (© Maxar Technologies) image from 4 August. Arrows point to zoomed in areas outlined by rectangles.

the dGPS base station set up in the same location every year using Trimble Geomatics 1.63 software. Base station points were further post processed using Natural Resource Canada's Canadian Spatial Reference System Precise Point Positioning (CSRS-PPP) online tool (http://www.nrcan.gc.ca/earth-sciences/geomatics/geodetic-reference-systems/tools-applications/10925#ppp). Survey markers and headwall positions were mapped and analyzed using ESRI ArcGIS v. 10.2.

Daily Weather Data

We used historical daily temperature and precipitation data from the Eureka Weather Station (http://climate.weather.gc.ca/climate_data/daily_data_e.html?StationID=50737). Eureka experiences a temperature inversion in coastal areas (Lesins et al., 2010) below approximately 60 m asl. Prior to February 2016, all air temperature measurements were recorded at the weather station located at 10 m asl. Beginning in February 2016, additional air temperature sensors were installed at the Eureka airstrip at 82 m asl. Air temperature measurements

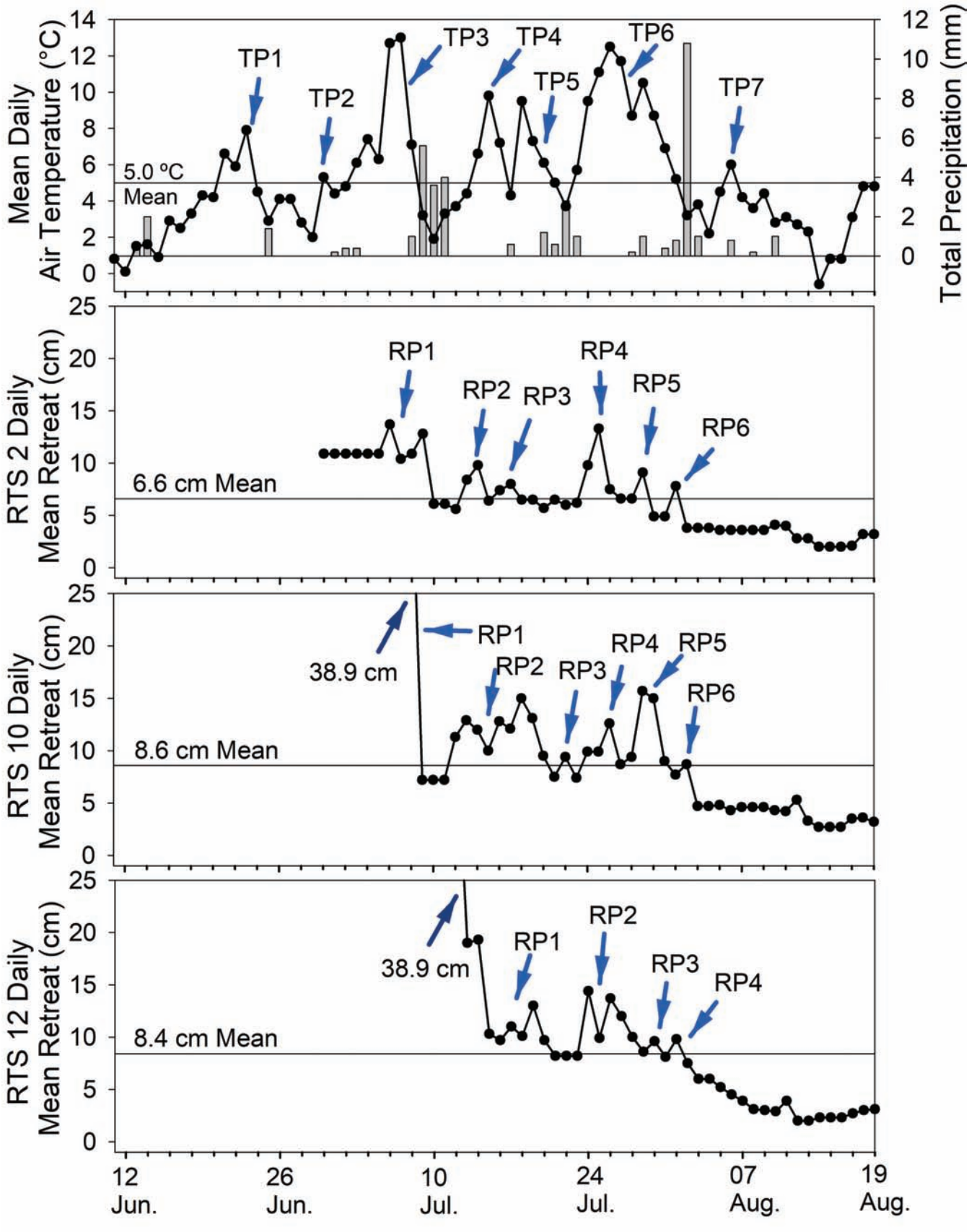

FIG. 3. Top graph shows mean daily air temperature and total daily precipitation before and during the monitoring period. Temperature peaks (TP) show periods of increased temperature above mean temperature for the consisted time period. Bottom three graphs show mean daily and overall mean retreat. Retreat peaks (RP) denote periods of increased retreat greater than the overall mean retreat.

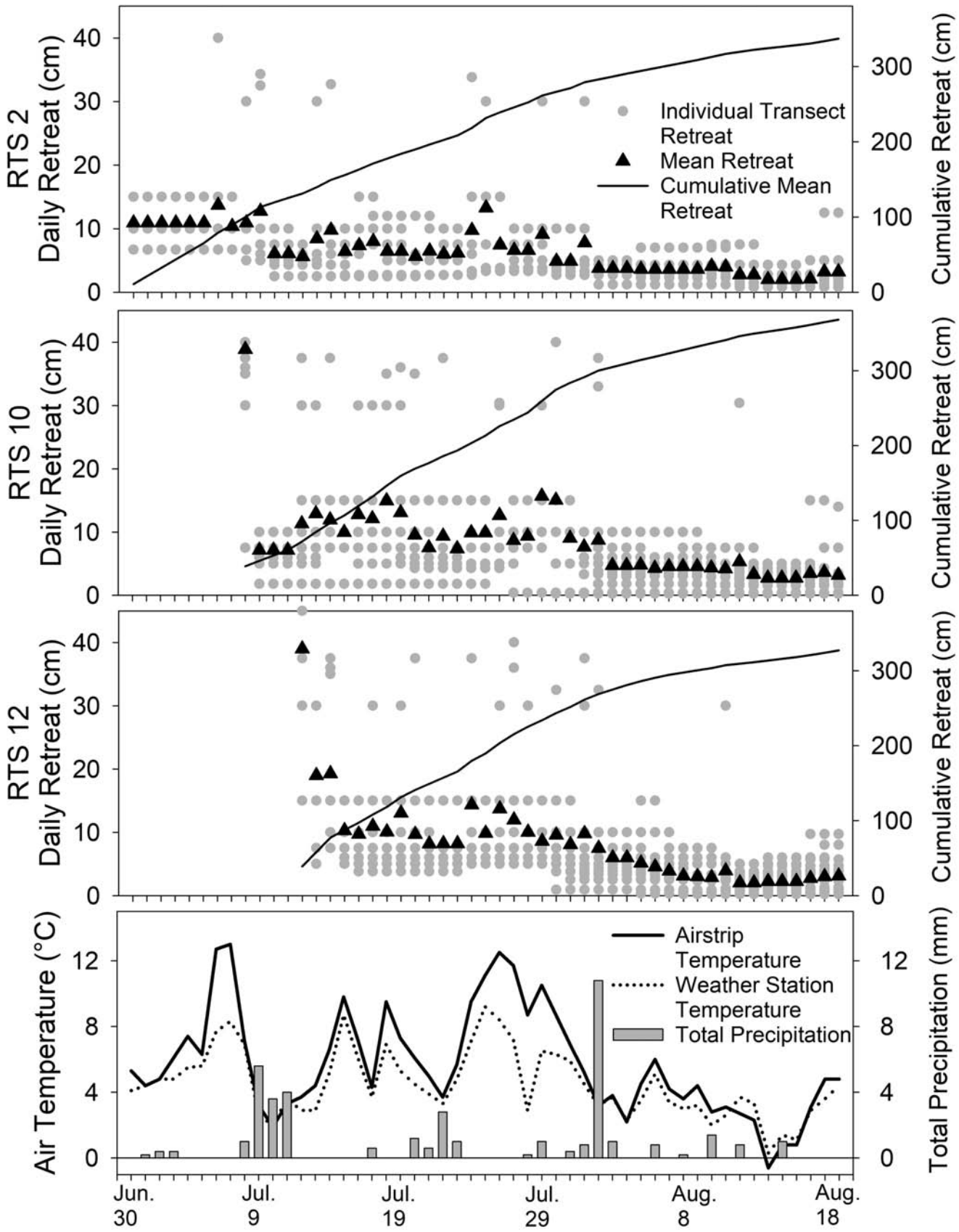

FIG. 4. Top three graphs show 2017 daily and mean cumulative retreat for each RTS site. Light gray circles show measured retreat at each survey transect, black triangles show the calculated mean daily retreat, and the black line shows the mean cumulative retreat using the mean daily retreat. Bottom graph shows mean daily air temperature and total daily precipitation. Air temperatures recorded both above (airstrip) and below (weather station or WS) the temperature inversion are included.

recorded below the inversion follow the same trends as those recorded above the inversion but are generally up to 4°C cooler (Grom and Pollard, 2008; Fig. 4). Ward Jones et al. (2019) assessed RTS activity between 1989 and 2018 and therefore used the station's record measured below the inversion. This study uses the air temperature record measured above the inversion during 2017. TDD patterns were determined using mean daily air temperature for each monitoring period for each RTS site. We denote temperature peaks (TP) as periods of increased temperature above the seasonal mean temperature (Fig. 3).

Sky condition observations obtained by the Eureka Weather Station (Table 2) were used as a proxy for total direct solar radiation during our monitoring period. Sky observation data are provided every two hours; we use the mode observation for the overall sky condition for each day. We assume that the clearer the sky (less cloud cover), the greater the amount of solar radiation each RTS is receiving within a given day.

Statistical Analyses

We explore statistical correlations between mean daily and mean cumulative RTS retreat with MDAT, total daily precipitation, and TDD with each individual RTS. To ensure data normality and constant variance, log transformations were done for certain statistical runs. Linear regression was the first statistical analysis performed. If data did not satisfy normality and constant variance, polynomial regression was then used (quadratic and then cubic). If normality and constant variance were still not satisfied, correlations were determined using Pearson correlation.

RESULTS

Daily Monitoring

RTS 2 was monitored the longest of all three sites. Monitoring consisted of 52 days (29 June – 19 August), spanning 68% of the thaw season (11 June – 27 August). RTS 2 experienced the lowest retreat rates compared to the other two sites, with weekly rates never surpassing 13.75 cm (Fig. 2). Retreat rates of 30 cm or greater occurred intermittently on 9, 13, 14, 24, and 25 July. Mean daily retreat ranged between 4.9 cm to 13.3 cm per day between 29 June and 1 August with six retreat peaks (RP; Fig. 3) and then shifted to between 2.0 cm and 4.1 cm/day from 2 to 19 August. Retreat peaks (Fig. 3) occurred on 29 June – 9 July (max. retreat during this period was 13.7 cm on 6 July), 13 – 14 July (9.8 cm on 14 July), 16 – 17 July (8.0 cm on 17 July), 24 – 26 July (13.3 cm on 25 July), 29 July (9.1 cm), and 1 August (7.8 cm). Overall mean retreat was 6.6 cm/day. Mean cumulative retreat was 337 cm. Cumulative retreat for each transect ranged from 261.3 cm to 385.4 cm.

Monitoring of RTS 10 spanned 43 days (8 July to 19 August) or 53% of the thaw season. Mean daily retreat ranged between 7.1 cm and 15.7 cm (not including the maximum retreat of 38.9 cm on 8 July) between 9 July and 2 August with six retreat peaks occurring during that

TABLE 2. Mode daily sky condition observations, mean daily retreat for each site, and mean daily air temperature from the Eureka Weather Station during the 2017 monitoring period. For days on which rain was the dominant sky condition, rain amount was also included.

Date	Mean retreat RTS 2/RTS 10/RTS 12 (cm)	MAT (˚C)	Mode weather observation	Date	Mean retreat RTS 2/RTS 10/RTS 12 (cm)	MAT (˚C)	Mode weather observation
29 June	NA/NA/NA	2.0	Mostly cloudy	25 July	13.3/9.9/9.9	11.1	Mainly clear
30 June	10.9/NA/NA	5.3	Mostly cloudy	26 July	7.5/12.6/13.7	12.5	Mostly cloudy
1 July	10.9/NA/NA	4.4	Cloudy	27 July	6.6/8.7/12.0	11.7	Mostly cloudy
2 July	10.9/NA/NA	4.8	Mostly cloudy	28 July	6.6/9.4/10.0	8.7	Mostly cloudy
3 July	10.9/NA/NA	6.1	Mostly cloudy	29 July	9.1/15.7/8.6	10.5	Mostly cloudy
4 July	10.9/NA/NA	7.4	Mostly cloudy	30 July	4.9/15.0/9.6	8.7	Cloudy
5 July	10.9/NA/NA	6.3	Mostly cloudy	31 July	4.9/9.0/8.1	6.9	Mostly cloudy
6 July	13.7/NA/NA	12.7	Mainly clear	1 Aug.	7.8/7.7/9.8	5.2	Mostly cloudy
7 July	10.4/NA/NA	13.0	Clear	2 Aug.	3.8/8.7/7.5	3.2	Rain (10.8 mm)
8 July	10.9/38.9/NA	7.1	Mostly cloudy	3 Aug.	3.8/4.7/6.0	3.8	Mostly cloudy
9 July	12.8/7.2/NA	3.2	Rain (1 mm)	4 Aug.	3.8/4.7/6.0	2.2	Mainly clear
10 July	6.1/7.2/NA	1.9	Rain (5.6 mm)	5 Aug.	3.6/4.8/5.2	4.5	Mainly clear
11 July	6.1/7.2/NA	3.3	Rain (3.6 mm)	6 Aug.	3.6/4.3/4.5	6.0	Mostly cloudy
12 July	5.6/11.3/39.0	3.7	Mostly cloudy	7 Aug.	3.6/4.6/3.9	4.2	Cloudy
13 July	8.4/12.9/19.0	4.4	Mostly cloudy	8 Aug.	3.6/4.6/3.1	3.6	Cloudy
14 July	9.8/12.0/19.3	6.6	Mainly clear	9 Aug.	3.6/4.6/3.0	4.4	Mostly cloudy
15 July	6.4/10.0/10.3	9.8	Mostly cloudy	10 Aug.	4.1/4.3/2.9	2.8	Cloudy
16 July	7.4/12.8/9.7	7.2	Mostly cloudy	11 Aug.	4.0/4.2/3.9	3.1	Mostly cloudy
17 July	8.0/12.1/11.0	4.3	Mainly clear	12 Aug.	2.8/5.5/2.0	2.7	Mostly cloudy
18 July	6.5/15.0/10.1	9.5	Mainly clear	13 Aug.	2.8/3.3/2.0	2.3	Mainly clear
19 July	6.5/13.1/13.0	7.3	Mostly cloudy	14 Aug.	2.0/2.7/2.3	−0.6	Mostly cloudy
20 July	5.7/9.5/9.7	6.1	Mostly cloudy	15 Aug.	2.0/2.7/2.3	0.8	Cloudy
21 July	6.5/7.5/8.2	5.0	Rain (0.6 mm)	16 Aug.	2.0/2.7/2.3	0.8	Clear
22 July	6.0/9.4/8.2	3.7	Rain (2.8 mm)	17 Aug.	2.1/3.5/2.7	3.1	Clear
23 July	6.2/7.4/8.2	5.7	Rain (1.0 mm)	18 Aug.	3.2/3.6/3.0	4.8	Mostly cloudy
24 July	9.8/9.9/14.4	9.5	Mostly cloudy	19 Aug.	3.2/3.2/3.1	4.8	Mostly cloudy

time (Fig. 3). Retreat peaks occurred on 8 July (38.9 cm), 12–20 July (max retreat during this period was 12.9 cm on 13 July), 22 July (9.4 cm), 24–26 July (12.6 cm on 26 July), 28–21 July (15.7 cm on 29 July), and 2 August (8.7 cm) within five periods of peak retreat. After 2 August, mean daily retreat ranged from 2.7 cm to 4.8 cm until the end of the monitoring period. Mean daily retreat for the entire monitoring period was 8.6 cm. This site experienced a series of rapid retreat at individual transects on 30 and 31 July, where five transects retreated 30 cm on 30 July (transects 4, 5 6, 7, and 11) and three others retreated 40 cm on 31 July (transects 1, 9, and 10). On 2 August, the day with the most rain of the study period (10.8 mm), two transects retreated 33 cm and 37.5 cm, respectively. Other rapid retreat events occurred on 13, 14, 17–22, 26 July and 3 and 12 August. Cumulative retreat ranged between 70.6 cm and 422.1 cm, and mean cumulative retreat was 329.0 cm.

Monitoring of RTS 12 was the shortest of all three sites, consisting of 39 days or 51% of the thaw season (12 July to 19 August). Mean daily retreat ranged from 7.5 cm to 19.3 cm between 13 July and 2 August (not including the maximum retreat of 39 cm on 12 July) (Fig. 3). Retreat peaks occurred on 12–20 July (max. retreat during this period was 39 cm on 12 July), 24–28 July (14.4 cm on 24 July), July 30 (9.6 cm), and 1 August (9.8 cm). Mean daily retreat between 3 and 19 August ranged between 2.0 cm and 6.0 cm. Mean daily retreat for the entire monitoring period was 8.4 cm. On the first day of monitoring (12 July), 19 of the 20 transects had retreat of 30 cm or more. On the second day (13 July), five transects retreated 30 cm or more, and the next day four transects retreated 30 cm or more. Other days with rapid retreat events included 14, 19, 23, 25–27, 30 July, and 1 and 2 August. Mean cumulative retreat was 327.2 and ranged between 198.9 cm and 466.8 cm.

Observations of RTS Floor Controls on RTS Retreat

Although difficult to quantify, the daily images taken of each RTS during each visit highlight the importance of terrain factors such as sediment distribution in the RTS floor on RTS retreat. RTS 10 and 12 had a developed network of gullies along the slump floor that consistently evacuated surface water from slumped sediments. These gullies have been present since at least 2014 according to field photos. In 2017, we observed that sediments would slump off the retreating headwall and accumulate along the base of the headwall in front of the ice face (Fig. 5). Sediments accumulated until a critical point was reached; between monitoring visits on 26 July and 27 July for both S10 and S12, these sediments suddenly were transported laterally along the perimeter of the headwall, leaving a greater area of ground ice exposed where the sediments originated prior to movement (Fig. 5). Furthermore, these sediments accumulated along the flanks of the RTS, leading to a small area of ground ice no longer being exposed. For RTS 2, a sediment lobe or tongue flowed down the valley. As sediments and water accumulated, the sediment lobe surged forward down the valley between 27 and 28 July (Fig. 5). All three sites experienced an increase in mean retreat immediately after these rapid sediment transport events.

Daily Weather

The 2017 thaw season was uncharacteristically wet with 23 rain events occurring throughout the study period with rainfall amounts ranging from 0.2 mm (occurring on 1 and 28 July and 8 August) to 10.8 mm (2 August; Figs. 3 and 4; Table 2). By analyzing the Eureka meteorological records between 1989 and 2018, we found that 2017 had the fourth highest amount of rain (Ward Jones et al., 2019). When comparing TDD between 1989 and 2018, 2017 was the fourth coolest summer. Mean daily air temperatures ranged from −0.6˚C (14 August) to 13.0˚C (7 July) and were characterized by seven temperature peaks (TP; Fig. 3) occurring on 6–7 July (TP3: 12.7˚C to 13.0˚C), 15 July (TP4: 9.8˚C), 18 July (TP5: 9.5˚C), 24–30 July (TP6: max temperature reached was 12.5˚C), and 6 August (TP 6: 6˚C). Mean monthly air temperatures for June, July, and August were 1.1˚C, 7.2˚C, and 2.4˚C, respectfully. Sky conditions were more frequently overcast than is characteristic of this area. During the study period there were three clear days, eight mainly clear days, 28 mostly cloudy days, and six cloudy days (Table 2).

Statistical Analyses

Mean daily retreat and cumulative retreat were statistically significant with both MDAT and TDD for all three RTSs (Table 3). RTS 2 had an adjusted R^2 of 0.375 and 0.626 when correlating mean daily retreat with MDAT ($p < 0.001$) and TDD ($p < 0.001$), respectively, using linear regression. Using quadratic regression, RTS 2 had an adjusted R^2 of 0.9964 when correlating cumulative retreat with TDD ($p < 0.0001$) and RTS 10 had an adjusted R^2 of 0.9959 ($p < 0.0001$). Using cubic regression, RTS 12 had an adjusted R^2 of 0.9980 ($p < 0.0001$) when correlating mean cumulative retreat with TDD. None of the RTSs had a statistically significant relationship between mean daily or mean cumulative retreat and total daily precipitation using Pearson correlation.

DISCUSSION

RTS Retreat Dynamics and Variables Impacting RTS Retreat

The complexity of RTS behaviour stems from a series of interacting variables that impact headwall retreat. These include solar radiation (Lewkowicz, 1986; Grom and Pollard, 2008), weather or climate variables such as

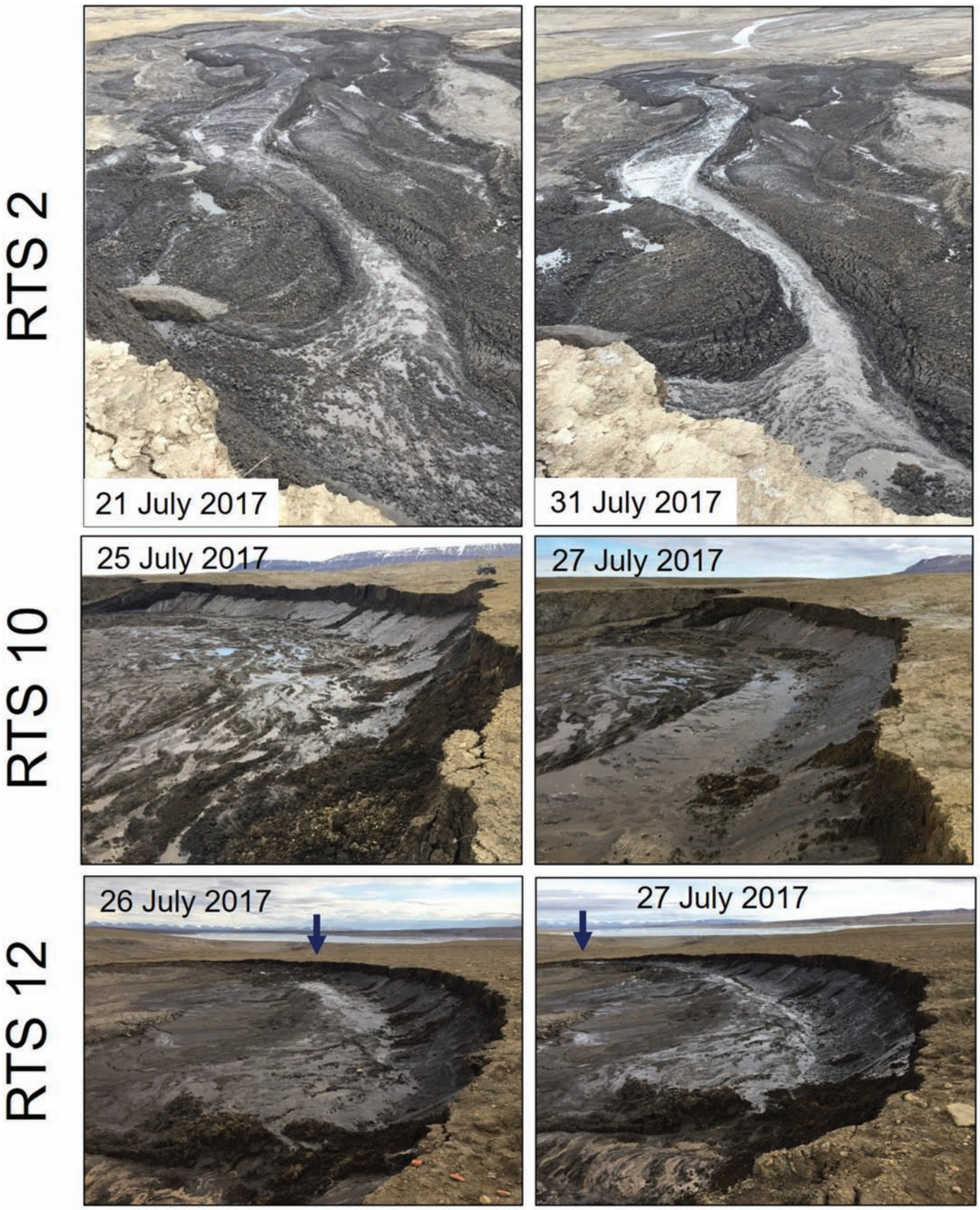

FIG. 5. Before and after photos of the largest sediment movement event during the monitoring period, images shown provide the best perspective. Sediments surged forward in a debris lobe along the RTS floor for RTS 2 between 27 and 28 July. Sediments were transported laterally along the headwall for both RTS 10 and RTS 12 (arrow points to edge of sediment accumulation) between 26 and 27 July.

TABLE 3. Summary of results of statistical correlation between either mean daily retreat (MDR in cm) or mean cumulative retreat (MCR in cm) and either mean daily air temperature (MDAT in ˚C), total daily precipitation (TDP in mm), or thawing degree days (TDD). Statistical techniques used were linear, quadratic, and cubic regression and Pearson correlation. Log transformations were used in certain statistical runs to maintain constant variance and data normality. Statistically significant *p* values are indicated in bold type.

Site (# of days monitored)	Variables	Statistical test[1]	Adjusted R^2	*p* value[2]	Correlation coefficient	Standard error of estimate
RTS 2 (n = 52)	1) Log MDR	Linear regression	0.375	< **0.001***	y_0 = 0.503	
	2) MDAT				a = 0.0454	0.186
	1) MDR	Pearson correlation	N/A	0.941	0.0106	N/A
	2) TDP					
	1) Log MDR	Linear regression	0.626	< **0.001***	y_0 = 2.819	0.144
	2) Log TDD				a = −0.888	
	1) MCR	Pearson correlation	N/A	**0.0236****	−0.317	N/A
	2) MDAT					
	1) MCR	Pearson correlation	N/A	0.741	−0.0474	N/A
	2) TDP					
	1) MDR	Quadratic regression	0.9964	**< 0.0001***	y_0 = 6.7035	5.9222
	2) TDD				a = 1.9812	
					b = −0.0024	
RTS 10 (n = 43)	1) MDR	Pearson correlation	N/A	**< 0.001***	0.499	
	2) MDAT					N/A
	1) MDR	Pearson correlation				
	2) TDP		N/A	0.898	0.0201	N/A
	1) Log MDR	Linear regression	0.403	**< 0.001***	y_0 = 2.232	0.196
	2) Log TDD				a = −0.196	
	1) MCR	Pearson correlation				
	2) MDAT		N/A	**0.0531*****	−0.297	N/A
	1) MCR	Pearson correlation				
	2) TDP		N/A	0.184	−0.206	N/A
	1) MCR	Quadratic regression	0.9959	**< 0.0001***	y_0 = 16.5755	6.8047
	2) TDD				a = 1.7693	
					b = −0.0014	
RTS 12 (n = 39)	1) MDR	Pearson correlation		**0.0250****		
	2) MDAT		N/A		0.359	N/A
	1) MDR	Pearson correlation		0.813		
	2) MTP		N/A		−0.0391	N/A
	1) log MDR	Linear regression	0.633	**< 0.001***	y_0 = 2.169	0.191
	2) log TDD				a = −0.673	
	1) MCR	Pearson correlation				
	2) MDAT		N/A	**0.00417***	−0.449	N/A
	1) MCR	Pearson correlation				
	2) TDP		N/A	0.646	0.0760	N/A
	1) MCR	Cubic regression			y_0 = 33.0502	
	2) TDD		0.9980	**< 0.0001***	a = 2.0993	3.3934
					b = −0.0065	
					c = 1.4319E-05	

[1] Linear formula: $y = y_0 + a*x$; quadratic formula: $y = y_0 + a*x + b*x^2$; cubic formula: $y = y_0 + a*x + b*x^2 + c*x^3$

[2] $p < 0.01$; ** $p < 0.05$; *** $p < 0.1$

air temperature (Kokelj et al., 2017; Lewkowicz and Way, 2019), TDD (Heginbottom, 1984; Robinson, 2000; Swanson and Nolan, 2018; Ward Jones et al., 2019), and precipitation (Kokelj et al., 2015; Segal et al., 2016) as well as terrain variables including RTS geometry (Lewkowicz, 1987), headwall heights (Wang et al., 2016), and slope (Lacelle et al., 2015; Swanson and Nolan, 2018; Ward Jones et al., 2019). All three RTS sites show a general pattern of varying retreat rates during the month of July to suddenly lower rates in August. There were five temperature peaks during the monitoring period, RTS 2 and RTS 10 each had six retreat peaks and RTS 12 had four (Fig. 3). We believe sediment evacuation is a major control of retreat peaks in addition to air temperature. Sediment distribution along the RTS floor may explain why each RTS experiences more than one retreat peak during a single temperature peak, and not all temperature peaks align with retreat peaks (Fig. 3). Sediments must be evacuated to expose the ice-rich headwall, hence the slope of the slump floor is important. The importance of slump floor slope was particularly apparent when a large pulse of sediments was transported laterally along the RTS floor in RTS 10 and RTS 12 (Fig. 5), as both experienced an immediate increase in mean retreat (Figs. 3 and 4). RTS 2 also experienced an increase in mean retreat when its debris tongue surged forward (Fig. 5).

The decreased retreat rates in August occurred almost simultaneously among all three RTS sites. Retreat rates decreased suddenly on 2 August at RTS 2 and on 3 August at RTS 10 (rates dropped approximately 4.0 cm for both sites), then remained fairly constant until the end of the

monitoring period (between 2.0 cm and 4.1 cm for RTS 2 and between 2.7 cm and 5.3 cm for RTS 10). Rates for RTS 12 decreased steadily from 9.6 cm on 1 August to 2.9 on 10 August and then ranged between 2.1 cm and 3.9 cm until 19 August. It is unclear why retreat rates decreased suddenly. Although there was one more temperature peak on 6 August, air temperatures never increased above 6.0˚C. Maximum active layer thaw depths were reached between 5 and 10 August (Ward Jones et al., 2020). The 6.0˚C air temperature may represent a threshold necessary for increased rates of retreat or there was insufficient solar radiation as mean total solar radiation decreased over the course of the study period. The high latitude and corresponding low solar declination and sun angle may be significant and may no longer contribute to RTS retreat after a certain date.

Solar radiation was regarded previously as a key factor in driving ground ice ablation and RTS retreat (Lewkowicz, 1986, 1987; Robinson, 2000; Grom and Pollard, 2008), but recent observations suggest solar radiation may play a less important role as higher rates of retreat tend to be achieved later in the thaw season (July) when the amount of potential solar radiation is decreasing. Zwieback et al. (2018) demonstrated that sub-seasonal retreat of RTSs in the Tuktoyaktuk Coastlands, Canada, and Bykovsky Peninsula, Russian Federation, were not energy limited during the thaw season, with the greatest divergence occurring in the early part of the thaw season. Swanson and Nolan (2018) report the same trends for RTSs in the Noatak Valley, Alaska. Our study also supports this finding, as the highest rates of retreat (particularly for RTS 2) occurred later in the thaw season when overall solar radiation was less. Overall, we do not think solar radiation has a dominant impact on retreat (because we lacked direct measurements this observation is anecdotal) since there were so few days of clear skies—only three clear and eight mainly clear days comprising 6% and 15% of the 52 monitoring days. In Eureka, however, the warmest days tend to have the clearest skies, and solar radiation may be more impactful during seasons with clearer skies. Lewkowicz (1986) found that on overcast days sensible and latent heat fluxes supplied more than half of the energy for headwall ablation. Furthermore, if RTS activity was critically linked to solar radiation, this would be reflected in RTS orientation, as the more direct sunlight an RTS receives, the greater its retreat should be. However, recent studies have shown that RTS orientation may be more important in RTS initiation but not in maintaining active RTSs (Wang et al., 2009; Lacelle et al., 2015; Khomutov et al., 2017; Ward Jones et al., 2019). The RTS with the most retreat (of 22 RTSs) monitored by Swanson and Nolan (2018) in the Noatak Valley, Alaska, was north facing. The majority of RTS sites that initiated in the Beiluhe Region of the Qinghai-Tibet Plateau, China, were on NE-facing slopes (Luo et al., 2019). RTS 12 is east facing and experienced the greatest mean cumulative retreat between 2011 and 2018 compared to RTS 2 and RTS 10 (Table 1; Ward Jones et al., 2019). Observations by Turner et al. (2021) found RTS retreat may be linked to solar radiation when assessing sub-seasonal retreat based on transects that align with sun azimuth angles, but overall retreat was observed to be the greatest during the highest air temperatures experienced during the study period.

Many studies have shown links between increased RTS initiation and retreat rates with increased air temperatures (Lantz and Kokelj, 2008; Kokelj et al., 2017; Lewkowicz and Way, 2019; Ward Jones et al., 2019). MDAT correlated with daily mean retreat in each statistical run for each site. When we used linear regression to correlate mean daily retreat with MDAT and TDD, RTS 2 had adjusted R^2 values of 0.375 for daily MAT and 0.626 for TDD. Armstrong et al. (2018) also had a higher R^2 value for TDD (0.73) than MDAT (0.62). All RTS sites had a statistically significant relation between mean daily retreat and TDD. Furthermore, all sites had adjusted R^2 values greater than 0.99 when correlating cumulative retreat with TDD. Quadratic regression was used for RTSs 2 and 10, whereas cubic regression was used for RTS 12. TDD has also been highly correlated to retreat in other studies. Swanson and Nolan (2018) had R^2 values using quadratic regression ranging between 0.971 and 1.000 for TDD and retreat of the centre position of the RTS headwall and R^2 values ranging from 0.982 to 1.000 for TDD, and RTS area growth for RTSs in Alaska. Robinson (2000) had R^2 values between 0.68 and 0.97 for midseason headwall retreat and TDD using linear regression for RTSs at Hot Weather Creek, also on the Fosheim Peninsula on Ellesmere Island. Heginbottom (1984) had R^2 values of 0.73 and 0.94 for mean and maximum retreat, respectively, for an RTS on Melville Island.

Currently, there has only been an observed increase in RTS retreat due to precipitation in the lower Arctic (Kokelj et al., 2015; Segal et al., 2016; Zwieback et al., 2018). Precipitation impacts RTS retreat by adding moisture to aid sediment transport along the RTS floor and in debris tongues as well as by reducing soil strength by increasing soil moisture (Kokelj et al., 2015; Zwieback et al., 2018), however surface runoff was observed to preferentially flow into the gully system that formed by 2014 at RTS 10 and 12. Ward Jones et al. (2019) found no correlation between precipitation and RTS retreat on an annual basis. We found no statistically significant correlation between precipitation and mean daily or mean cumulative retreat. The highest amount of rainfall occurred on 2 August (10.8 mm). Although this locally impacted a few transects, including a gully that formed in the ice face of a transect at RTS 10, there was no overall observed increase in mean retreat that day or in the few days after. Kokelj et al. (2015) found rain events that were 30 mm or greater to be impactful. Being a polar desert, Eureka simply does not experience rainfall events of that magnitude.

Like climate and weather variables, terrain variables provide an important control on RTS activity and include aspect, ground ice conditions, RTS morphology, headwall height, slope, and slumped sediments along the RTS floor. Whereas weather variables are experienced fairly equally

within a certain area, terrain variables can exhibit a high degree of heterogeneity leading to contradictory research results between studies (Swanson and Nolan, 2018). Lacelle et al. (2015) found a statistically significant correlation with aspect, but Wang et al. (2016), Swanson and Nolan (2018), Zwieback et al. (2018), and Ward Jones et al. (2019) did not.

Studies have shown that areas with higher ground ice content are more likely to have RTS development (e.g., Kokelj et al., 2017; Ramage et al., 2017). Ground ice conditions can only be attained with detailed field surveys and, although there is an effort to model ground ice conditions at a larger scale (O'Neill et al., 2019), there is still uncertainty across the Arctic, and resolutions are coarse (1 km^2). Swanson and Nolan (2018) suggest both ground ice content and slope controls RTS growth rates, however, RTS 12 had lower volumetric ground ice than the other two sites but had retreated the most among the 12 sites discussed in Ward Jones et al. (2019).

The ability of an RTS to evacuate sediments is critical in maintaining active RTSs. In areas with insufficient precipitation to be impactful on retreat, such as our study area that is located in a polar desert, the main moisture input is directly from the ice face and is dependent on ground ice content. Therefore, sediment input amounts (by an RTS's overburden and sediment within ground ice) and slope may be more critical factors in sediment evacuation at our site than in areas with greater precipitation amounts. These variables would be particularly important to evacuate the sediment buildup that triggered the sediment pulse at all three sites at the end of July. Although Robinson (2000) found the fastest retreat at RTS with a terrain slope (> 10˚) and Swanson and Nolan (2018) found the highest retreat on moderate slopes (~14% or ~8˚), our three RTS sites have lower slopes at 5.2˚ for RTS 2, 1.3˚ for RTS 10, and 1.6˚ for RTS 12. Ward Jones et al. (2019) found RTSs with the lowest slopes to be the most active and that taking the ratio of slope of undisturbed terrain to the slope of the slump floor was a good indicator of RTS activity. RTSs with a ratio above 1 tended to be the most active, likely because the ratio indicated which RTSs had ideal slopes for sediment evacuation. Recent advancements in using remotely piloted aircraft systems (e.g., Van der Sluijs et al., 2018; Turner et al., 2021), terrestrial laser scanners (e.g., Barnhart and Crosby, 2013), and structure for motion photography (e.g., Armstrong et al., 2018) may provide opportunities to study the dynamics of the RTS floor and better understand the impacts on RTS retreat.

TDD, Cumulative Retreat, and Retreat Modelling

Swanson and Nolan (2018) suggested the high correlation of TDD could be used to predict growth for individual RTS. We tested this hypothesis with RTS 10 and RTS 12 for sub-seasonal observations by monitoring these two sites for two weeks during the 2018 season (6–21 July). Mean retreat for RTS 10 and RTS 12 was 110 cm and 132 cm, respectively, and TDD during this time was 74.2. We did not monitor RTS 2 because there was no longer ground ice exposed, and therefore it was considered inactive. Using the quadratic regression equation for cumulative retreat and TDD for RTS 10 (Table 3), we inputted TDD for the 2018 monitoring period to predict cumulative retreat. The regression equation resulted in a cumulative retreat of 128 cm and giving a percent prediction error (PPE) between the predicted and measured value of 16%. Repeating for the cubic regression equation for RTS 12 yielded a prediction cumulative retreat value of 122 cm and a PPE of 8%.

The high correlations between retreat and TDD can be successfully used to model and estimate future RTS growth. However, these estimations have largely been confined to a single RTS site or a few occurring in an area (Robinson, 2000; Swanson and Nolan, 2018). Swanson and Nolan (2018) had high R^2 values using quadratic curves and estimated RTS growth rate using TDD with low PPE of 1.4%. They also developed a linear model to estimate the growth rate of an RTS using TDD and slope of the undisturbed surface. Wang et al. (2016) provided a quadratic regression equation using headwall height. Lewkowicz (1987) modelled headwall retreat using an equation consisting of weather variables and RTS geometry.

Although many factors impact RTS retreat including solar radiation and climate and terrain variables, TDD and cumulative retreat correlate so highly because both variables account for lag retreat responses and past and present conditions throughout the thaw season, whereas mean daily retreat and MDAT only account for present-day conditions. The use of TDD and cumulative retreat allows for accurate modelling with less detailed data collection required for model inputs, as only air temperature and headwall position are needed, and the later could be acquired using remote sensing.

CONCLUSION

This study monitored three retrogressive thaw slumps at a sub-seasonal scale to gain additional insights into RTS dynamics and explored statistical correlations using daily mean and cumulative retreat and MDAT, total daily precipitation, and TDD to help inform future research efforts. Our observations and analysis support the following conclusions:

1) TDD can explain almost all of the variation (R^2 > 0.99) in cumulative retreat for all sites, likely because both variables account for past and present conditions throughout the thaw season, including lags responses of headwall retreat. These variables (total cumulative retreat and total cumulative TDD) can be used to model the next season's retreat for individual RTS sites at sub-seasonal scales.
2) MDAT and TDD yielded statistically significant relationships with mean daily and cumulative retreat at all three sites.

3) There was no statistically significant relationship between total precipitation and either mean daily or cumulative retreat. Precipitation amounts in the Eureka area are likely insufficient to impact RTS retreat.
4) Our August retreat observations suggest an air temperature or solar radiation threshold must be reached for increased retreat rates.

With recent decadal observations of increased RTS numbers, rates, and size, understanding RTS activity is vital as these features impact vegetation communities, aquatic and terrestrial ecosystems through the release of solutes, and can impact local infrastructure. Detailed sub-seasonal observations are critical and needed for other parts of the Arctic as this scale of detailed data shows relationships and trends that can be obscured by observations at annual scales.

ACKNOWLEDGEMENTS

The length of time to monitor these three retrogressive thaw slumps would not have been possible without the Research Support Opportunity in Arctic Environmental Studies provided by the Association of Canadian Universities for Northern Studies awarded to M. Ward Jones. We thank the Eureka Weather Station staff for lodging and assistance during fieldwork. Polar Continental Shelf Program provided additional logistical field support. The Natural Sciences and Engineering Research Council of Canada provided funding for this research (awarded to W. Pollard). Additional student support for M. Ward Jones was provided by the Northern Scientific Training Program, the Fonds de Recherche du Quebec – Nature et Technologies doctoral scholarship, an Eben Hopson Fellowship and a David Erb Fellowship. Thank you to Cameron Roy, Fanny Amyot, Michael Templeton, and Dale Anderson for their assistance during fieldwork. We thank Benjamin Jones and Brian Moorman for reading earlier drafts of this manuscript and providing constructive comments. We thank two anonymous reviewers for their suggestions in improving this manuscript.

REFERENCES

Armstrong, L., Lacelle, D., Fraser, R.H., Kokelj, S., and Knudby, A. 2018. Thaw slump activity measured using stationary cameras in time-lapse and Structure-from-Motion photogrammetry. Arctic Science 4(4):827–845. https://doi.org/10.1139/as-2018-0016

Barnhart, T.B., and Crosby, B.T. 2013. Comparing two methods of surface change detection on an evolving thermokarst using high-temporal-frequency terrestrial laser scanning, Selawik River, Alaska. Remote Sensing 5(6):2813–2837. https://doi.org/10.3390/rs5062813

Becker, M.S., and Pollard, W.H. 2016. Sixty-year legacy of human impacts on a High Arctic ecosystem. Journal of Applied Ecology 53(3):876–884. https://doi.org/10.1111/1365-2664.12603

Becker, M.S., Davies, T.J., and Pollard, W.H. 2016. Ground ice melt in the High Arctic leads to greater ecological heterogeneity. Journal of Ecology 104(1):114–124. https://doi.org/10.1111/1365-2745.12491

Bernard-Grand'Maison, C., and Pollard, W. 2018. An estimate of ice wedge volume for a High Arctic polar desert environment, Fosheim Peninsula, Ellesmere Island. The Cryosphere 12(11):3589–3604. https://doi.org/10.5194/tc-12-3589-2018

Bowden, W.B., Gooseff, M.N., Balser, A., Green, A., Peterson, B.J., and Bradford, J. 2008. Sediment and nutrient delivery from thermokarst features in the foothills of the North Slope, Alaska: Potential impacts on headwater stream ecosystems. Journal of Geophysical Research: Biogeosciences 113(G2): G02026. https://doi.org/10.1029/2007JG000470

Burn, C.R. (2000). The thermal regime of a retrogressive thaw slump near Mayo, Yukon Territory. Canadian Journal of Earth Sciences 37(7):967–981. https://doi.org/10.1139/e00-017

Burn, C.R., and Lewkowicz, A.G. 1990. Canadian landform examples – 17 retrogressive thaw slumps. The Canadian Geographer 34(3):273–276. https://doi.org/10.1111/j.1541-0064.1990.tb01092.x

Couture, N.J., and Pollard, W.H. 2007. Modelling geomorphic response to climatic change. Climatic Change 85(3): 407. https://doi.org/10.1007/s10584-007-9309-5

Cray, H.A., and Pollard, W.H. 2015. Vegetation recovery patterns following permafrost disturbance in a Low Arctic setting: Case study of Herschel Island, Yukon, Canada. Arctic, Antarctic, and Alpine Research 47(1):99–113. https://doi.org/10.1657/AAAR0013-076

De Krom, V., and Pollard, W.H. 1989. The occurrence of ground ice slumps on Herschel Island, Yukon Territory. Musk-Ox 37:1–7.

Garneau, M. 2000. Peat accumulation and climatic change in the High Arctic. In: Garneau, M., and Alt, B.T., eds. Environmental response to climate change in the Canadian High Arctic. Geological Survey of Canada Bulletin 529. Ottawa: Natural Resources Canada. 283–293. https://doi.org/10.4095/211968

Grom, J.D., and Pollard, W.H. 2008. A study of High Arctic retrogressive thaw slump dynamics, Eureka Sound Lowlands, Ellesmere Island. In: Kane, D.L., and Hinkel, K.M., eds. Proceedings of the Ninth International Conference on Permafrost. 29 June–3 July 2008, University of Alaska Fairbanks. 545–550.

Grosse, G., Harden, J., Turetsky, M., McGuire, A.D., Camill, P., Tarnocai, C., Frolking, S., et al. 2011. Vulnerability of high-latitude soil organic carbon in North America to disturbance. Journal of Geophysical Research: Biogeosciences 116(G4): G00K06. https://doi.org/10.1029/2010JG001507

Günther, F., Grosse, G., Wetterich, S., Jones, B.M., Kunitsky, V.V., Kienast, F., and Schirrmeister, L. 2015. The Batagay mega thaw slump, Yana Uplands, Yakutia, Russia: Permafrost thaw dynamics on decadal time scale. PAST Gateways – Palaeo-Arctic Spatial and Temporal Gateways. Third International Conference and Workshop, 18–22 May 2015, Potsdam, Germany.

Harris, C., and Lewkowicz, A.G. 1993. Form and internal structure of active-layer detachment slides, Fosheim Peninsula, Ellesmere Island, Northwest Territories, Canada. Canadian Journal of Earth Sciences 30(8):1708–1714. https://doi.org/10.1139/e93-149

Heginbottom, J.A. 1984. Continued headwall retreat of a retrogressive thaw flow slide, eastern Melville Island, Northwest Territories. Current research: Part B, Geological Survey of Canada Paper 84-1B:363–365. https://doi.org/10.4095/119594

Hodgson, D.A., and Nixon, F.M. 1998. Ground ice volumes determined from shallow cores from western Fosheim Peninsula, Ellesmere Island, Northwest Territories. Geological Survey of Canada Bulletin 507. Ottawa: Natural Resources Canada. 178 p. https://doi.org/10.4095/209576

Khomutov, A., Leibman, M., Dvornikov, Y., Gubarkov, A., Mullanurov, D., and Khairullin, R. 2017. Activation of cryogenic earth flows and formation of thermocirques on central Yamal as a result of climate fluctuations. In: Mikoš, M., Vilímek, V., Yin, Y., and Sassa, K., eds. Advancing Culture of Living with Landslides, Fourth World Landslide Forum. Cham, Switzerland: Springer. 209–216. https://doi.org/10.1007/978-3-319-53483-1_24

Kokelj, S.V., and Jorgenson, M.T. 2013. Advances in thermokarst research. Permafrost and Periglacial Processes 24(2):108–119. https://doi.org/10.1002/ppp.1779

Kokelj, S.V., and Lewkowicz, A.G. 1999. Salinization of permafrost terrain due to natural geomorphic disturbance, Fosheim Peninsula, Ellesmere Island. Arctic 52(4):372–385. https://doi.org/10.14430/arctic942

Kokelj, S.V., Lacelle, D., Lantz, T.C., Tunnicliffe, J., Malone, L., Clark, I.D., and Chin, K.S. 2013. Thawing of massive ground ice in mega slumps drives increases in stream sediment and solute flux across a range of watershed scales. Journal of Geophysical Research: Earth Surface 118(2):681–692. https://doi.org/10.1002/jgrf.20063

Kokelj, S.V., Tunnicliffe, J., Lacelle, D., Lantz, T.C., Chin, K.S., and Fraser, R. 2015. Increased precipitation drives mega slump development and destabilization of ice-rich permafrost terrain, northwestern Canada. Global and Planetary Change 129:56–68. https://doi.org/10.1016/j.gloplacha.2015.02.008

Kokelj, S.V., Lantz, T.C., Tunnicliffe, J., Segal, R., and Lacelle, D. 2017. Climate-driven thaw of permafrost preserved glacial landscapes, northwestern Canada. Geology 45(4):371–374. https://doi.org/10.1130/G38626.1

Lacelle, D., Brooker, A., Fraser, R.H., and Kokelj, S.V. 2015. Distribution and growth of thaw slumps in the Richardson Mountains–Peel Plateau region, northwestern Canada. Geomorphology 235:40–51. https://doi.org/10.1016/j.geomorph.2015.01.024

Lantuit, H., and Pollard, W.H. 2008. Fifty years of coastal erosion and retrogressive thaw slump activity on Herschel Island, southern Beaufort Sea, Yukon Territory, Canada. Geomorphology 95(1-2):84–102. https://doi.org/10.1016/j.geomorph.2006.07.040

Lantz, T.C, and Kokelj, S.V. 2008. Increasing rates of retrogressive thaw slump activity in the Mackenzie Delta region, N.W.T., Canada. Geophysical Research Letters 35(6): L06502. https://doi.org/10.1029/2007GL032433

Lantz, T.C., Kokelj, S.V., Gergel, S.E., and Henry, G.H.R. 2009. Relative impacts of disturbance and temperature: Persistent changes in microenvironment and vegetation in retrogressive thaw slumps. Global Change Biology 15(7):1664–1675. https://doi.org/10.1111/j.1365-2486.2009.01917.x

Lesins, G., Duck, T.J., and Drummond, J.R. 2010. Climate trends at Eureka in the Canadian High Arctic. Atmosphere-Ocean 48(2):59–80. https://doi.org/10.3137/AO1103.2010

Lewkowicz, A.G. 1986. Rate of short-term ablation of exposed ground ice, Banks Island, Northwest Territories, Canada. Journal of Glaciology 32(112):511–519. https://doi.org/10.1017/S0022143000012223

———. 1987. Headwall retreat of ground-ice slumps, Banks Island, Northwest Territories. Canadian Journal of Earth Sciences 24(6):1077–1085. https://doi.org/10.1139/e87-105

———. 1990. Morphology, frequency and magnitude of active-layer detachment slides, Fosheim Peninsula, Ellesmere Island, N.W.T. In: Proceedings of the 5th Canadian Permafrost Conference, 6 June 1990, Centre d'études Nordiques, Université Laval, Québec City, Quebec. Collection Nordicana 54. 111–118.

———. 2007. Dynamics of active-layer detachment failures, Fosheim Peninsula, Ellesmere Island, Nunavut, Canada. Permafrost and Periglacial Processes 18(1):89–103. https://doi.org/10.1002/ppp.578

Lewkowicz, A.G., and Harris, C. 2005. Morphology and geotechnique of active-layer detachment failures in discontinuous and continuous permafrost, northern Canada. Geomorphology 69(1-4):275–297. https://doi.org/10.1016/j.geomorph.2005.01.011

Lewkowicz, A.G., and Way, R.G. 2019. Extremes of summer climate trigger thousands of thermokarst landslides in a High Arctic environment. Nature Communications 10(1): 1329. https://doi.org/10.1038/s4146

Liljedahl, A.K., Boike, J., Daanen, R.P., Fedorov, A.N., Frost, G.V., Grosse, G., Hinzman, L.D., et al. 2016. Pan-Arctic ice-wedge degradation in warming permafrost and its influence on tundra hydrology. Nature Geoscience 9(4):312–318. https://doi.org/10.1038/ngeo2674

Luo, J., Niu, F., Lin, Z., Liu, M., and Yin, G. 2019. Recent acceleration of thaw slumping in permafrost terrain of Qinghai-Tibet Plateau: An example from the Beiluhe region. Geomorphology 341:79–85. https://doi.org/10.1016/j.geomorph.2019.05.020

Malone, L., Lacelle, D., Kokelj, S., and Clark, I.D. 2013. Impacts of hillslope thaw slumps on the geochemistry of permafrost catchments (Stony Creek watershed, NWT, Canada). Chemical Geology 356:38–49. https://doi.org/10.1016/j.chemgeo.2013.07.010

Mesquita, P.S., Wrona, F.J., and Prowse, T.D. 2010. Effects of retrogressive permafrost thaw slumping on sediment chemistry and submerged macrophytes in Arctic tundra lakes. Freshwater Biology 55(11):2347–2358. https://doi.org/10.1111/j.1365-2427.2010.02450.x

Murton, J.B., Edwards, M.E., Lozhkin, A.V., Anderson, P.M., Savvinov, G.N., Bakulina, N., Bondarenko, O.V. 2017. Preliminary paleoenvironmental analysis of permafrost deposits at Batagaika megaslump, Yana Uplands, northeast Siberia. Quaternary Research 87(2):314–330. https://doi.org/10.1017/qua.2016.15

Obu, J., Lantuit, H., Grosse, G., Günther, F., Sachs, T., Helm, V., and Fritz, M. 2017. Coastal erosion and mass wasting along the Canadian Beaufort Sea based on annual airborne LiDAR elevation data. Geomorphology 293(Part B):331–346. https://doi.org/10.1016/j.geomorph.2016.02.014

O'Neill, H.B., Wolfe, S.A., and Duchesne, C. 2019. New ground ice maps for Canada using a paleogeographic modelling approach. The Cryosphere 13(3):753–773. https://doi.org/10.5194/tc-13-753-2019

Pollard, W.H. 2000. Distribution and characterization of ground ice on Fosheim Peninsula, Ellesmere Island, Nunavut. In: Garneau, M., and Alt, B.T., eds. Environmental response to climate change in the Canadian High Arctic. Geological Survey of Canada Bulletin 529. Ottawa: Natural Resources Canada. 207–233. https://doi.org/10.4095/211959

Pollard, W., and Bell, T. 1998. Massive ice formation in the Eureka Sound Lowlands: A landscape model. In: Proceedings of the 7th International Conference on Permafrost, 23–27 June 1998, Yellowknife, Northwest Territories. Collection Nordicana 55. 903–908.

Pollard, W., Ward, M., and Becker, M. 2015. The Eureka Sound lowlands: An ice-rich permafrost landscape in transition. GeoQuébec 2015: Proceedings of the 68th Canadian Geotechnical Conference and the 7th Canadian Permafrost Conference, 21–23 September 2015, Quebec City, Quebec.

Ramage, J.L., Irrgang, A.M., Herzschuh, U., Morgenstern, A., Couture, N., and Lantuit, H. 2017. Terrain controls on the occurrence of coastal retrogressive thaw slumps along the Yukon Coast, Canada. Journal of Geophysical Research: Earth Surface 122(9):1619–1634. https://doi.org/10.1002/2017JF004231

Robinson, S.D. 2000. Thaw-slump-derived thermokarst near Hot Weather Creek, Ellesmere Island, Nunavut. In: Garneau, M., and Alt, B.T., eds. Environmental response to climate change in the Canadian High Arctic. Geological Survey of Canada Bulletin 529. Ottawa: Natural Resources Canada. 335–345. https://doi.org/10.4095/211972

Roy, C. 2019. The origin of massive ground ice in raised marine sediments along the Eureka Sound Lowlands, Nunavut, Canada. MSc thesis, McGill University.

Segal, R.A., Lantz, T.C., and Kokelj, S.V. 2016. Acceleration of thaw slump activity in glaciated landscapes of the western Canadian Arctic. Environmental Research Letters 11(3): 034025. https://doi.org/10.1088/1748-9326/11/3/034025

Swanson, D.K. 2021. Permafrost thaw-related slope failures in Alaska's Arctic national parks, *c*. 1980–2019. Permafrost and Periglacial Processes (Early View). 15 p. https://doi.org/10.1002/ppp.2098

Swanson, D., and Nolan, M. 2018. Growth of retrogressive thaw slumps in the Noatak Valley, Alaska, 2010–2016, measured by airborne photogrammetry. Remote Sensing 10(7): 983. https://doi.org/10.3390/rs10070983

Thienpont, J.R., Rühland, K.M., Pisaric, M.F.J., Kokelj, S.V., Kimpe, L.E., Blais, J.M., and Smol, J.P. 2013. Biological responses to permafrost thaw slumping in Canadian Arctic lakes. Freshwater Biology 58(2):337–353. https://doi.org/10.1111/fwb.12061

Turner, K.W., Pearce, M.D., and Hughes, D.D. 2021. Detailed characterization and monitoring of a retrogressive thaw slump from remotely piloted aircraft systems and identifying associated influence on carbon and nitrogen export. Remote Sensing 13(2): 171. https://doi.org/10.3390/rs13020171

Van der Sluijs, J., Kokelj, S.V., Fraser, R.H., Tunnicliffe, J., and Lacelle, D. 2018. Permafrost terrain dynamics and infrastructure impacts revealed by UAV photogrammetry and thermal imaging. Remote Sensing 10(11): 1734. https://doi.org/10.3390/rs10111734

Wang, B., Paudel, B., and Li, H. (2009). Retrogression characteristics of landslides in fine-grained permafrost soils, Mackenzie Valley, Canada. Landslides 6(2):121–127. https://doi.org/10.1007/s10346-009-0150-y

Wang, B., Paudel, B., and Li, H. 2016. Behaviour of retrogressive thaw slumps in northern Canada – three-year monitoring results from 18 sites. Landslides 13(1):1–8. https://doi.org/10.1007/s10346-014-0549-y

Ward Jones, M.K., and Pollard, W.H. 2018. Daily monitoring of a retrogressive thaw slump on the Fosheim Peninsula, Ellesmere Island, Nunavut. 5th European Conference on Permafrost (EUCOP), 23 June – 1 July 2018, Chamonix-Mont-Blanc, France.

Ward Jones, M.K., Pollard, W.H., and Jones, B.M. 2019. Rapid initialization of retrogressive thaw slumps in the Canadian High Arctic and their response to climate and terrain factors. Environmental Research Letters 14(5): 055006. https://doi.org/10.1088/1748-9326/ab12fd

Ward Jones, M.K., Pollard, W.H., and Amyot, F. 2020. Impacts of degrading ice wedges on ground temperatures in a High Arctic polar desert system. Journal of Geophysical Research: Earth Surface 125(3): e2019JF005173. https://doi.org/10.1029/2019JF005173

Zwieback, S., Kokelj, S.V., Günther, F., Boike, J., Grosse, G., and Hajnsek, I. 2018. Sub-seasonal thaw slump mass wasting is not consistently energy limited at the landscape scale. The Cryosphere 12(2):549–564. https://doi.org/10.5194/tc-12-549-2018